JACS
JOURNAL OF THE AMERICAN CHEMICAL SOCIETY
Communication
pubs.acs.org/JACS

Single ^{19}F Probe for Simultaneous Detection of Multiple Metal Ions Using miCEST MRI

Amnon Bar-Shir,[†,‡] Nirbhay N. Yadav,[†,#] Assaf A. Gilad,[†,‡,#] Peter C. M. van Zijl,[†,#] Michael T. McMahon,[†,#] and Jeff W. M. Bulte*[,†,‡,#,§,∥,⊥]

[†]Russell H. Morgan Department of Radiology and Radiological Science, [‡]Cellular Imaging Section and Vascular Biology Program, Institute for Cell Engineering, [§]Department of Biomedical Engineering, [∥]Department of Chemical & Biomolecular Engineering, and [⊥]Department of Oncology, The Johns Hopkins University School of Medicine, Baltimore, Maryland 21205, United States

[#]F.M. Kirby Research Center for Functional Brain Imaging, Kennedy Krieger Institute, Baltimore, Maryland 21205, United States

Supporting Information

ABSTRACT: The local presence and concentration of metal ions in biological systems has been extensively studied *ex vivo* using fluorescent dyes. However, the detection of multiple metal ions *in vivo* remains a major challenge. We present a magnetic resonance imaging (MRI)-based method for noninvasive detection of specific ions that may be coexisting, using the tetrafluorinated derivative of the BAPTA (TF-BAPTA) chelate as a ^{19}F chelate analogue of existing optical dyes. Taking advantage of the difference in the ion-specific ^{19}F nuclear magnetic resonance (NMR) chemical shift offset ($\Delta\omega$) values between the ion-bound and free TF-BAPTA, we exploited the dynamic exchange between ion-bound and free TF-BAPTA to obtain MRI contrast with multi-ion chemical exchange saturation transfer (miCEST). We demonstrate that TF-BAPTA as a prototype single ^{19}F probe can be used to separately visualize mixed Zn^{2+} and Fe^{2+} ions in a specific and simultaneous fashion, without interference from potential competitive ions.

A major challenge in the biomedical sciences is to monitor, characterize, quantify, and understand the multiplexity of biological events *in vivo*. Advanced imaging methodologies are being developed to visualize multiple biological changes simultaneously within the same anatomical frame. One strategy is the use of multimodal imaging approaches, where more than one imaging methodology is used to obtain information from multiple targets.[1−6] However, the complexity of coregistering the obtained information into an accurate spatial representation calls for probing multiple targets using a single imaging approach.

Metal ions play a pivotal role in nearly all biological processes, and deviation from normal levels is often associated with disease onset and progression.[7] Today, our knowledge of the role of metal ions in biology is mostly based on the use of optical dyes,[8] originally developed by Roger Tsien.[9,10] Although optical dyes have made an enormous contribution to an understanding of the role of metal ions in biological systems, the optical signal from fluorescent dyes limits their applications to *in vitro* studies or monitoring of surface phenomena *in vivo* using superficially injected dyes.[11] To overcome these limitations, magnetic resonance imaging (MRI) has been explored as a whole-body, noninvasive imaging technique to sense changes in metal ion levels *in vivo*.[12−14] However, currently available probes are designed to alter the T_1 and T_2 proton relaxation rates upon binding to the metal ion of interest,[15−17] where interpreting images and quantifying local metal levels may be difficult as this approach is not specific: changes in T_1 or T_2 may result from other sources, while the background contrast without the presence of metals is often unknown. The specific chemical shifts ($\Delta\omega$) of nuclear magnetic resonance (NMR)-detectable nuclei (e.g., ^{19}F or ^{129}Xe) in a synthetic probe upon metal ion binding provide ultimate specificity with regard to the ion of interest.[18−21] Unfortunately, NMR spectroscopy-based approaches do not provide spatial information on the location of the investigated ion and rely on the identification and integration of a specific NMR peak that may fall below a detectable signal to noise ratio (SNR).

Chemical exchange saturation transfer (CEST) imaging[22−26] is an MRI contrast mechanism that enables the detection of low concentration solutes via the transfer of their magnetization to the bulk (high concentration) nuclei, from which the MRI signal is derived. Using ^{1}H as the bulk nucleus, CEST MRI has been used in a wide range of applications,[22−26] including simultaneous imaging of different probes, based on their different $\Delta\omega$ values.[27,28] In our previously suggested approach, which we termed ion CEST (iCEST),[29] a combination of ^{19}F MRI and CEST was used to spatially monitor Ca^{2+} with high specificity, capitalizing on the dynamic exchange between the ion-bound and free ^{19}F chelate, and the shift in the $\Delta\omega$ of ^{19}F upon ion binding. By using 5,5′,6,6′-tetrafluoro-BAPTA (TF-BAPTA) as the ^{19}F iCEST probe (Figure 1a), we demonstrate here that Zn^{2+} and Fe^{2+} ions can be detected specifically and simultaneously.

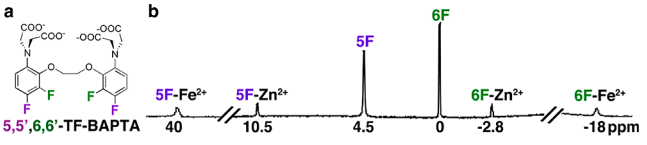

Figure 1. (a) Chemical structure of TF-BAPTA showing the ^{19}F atom substituents on the 5 (purple) and 6 (green) positions. (b) ^{19}F NMR spectrum (470 MHz) of 5 mM TF-BAPTA (20 mM Hepes buffer, pH = 7.2) in the presence of 0.5 mM Zn^{2+} or Fe^{2+}.

Received: November 4, 2014
Published: December 19, 2014

   dx.doi.org/10.1021/ja511313k | J. Am. Chem. Soc. 2015, 137, 78−81

It has been previously demonstrated that different ^{19}F-BAPTA derivatives have different $\Delta\omega$ values in their respective ^{19}F NMR spectra and variable K_d properties for various metal ions.[19] Because of the fact that free TF-BAPTA exchanges too rapidly ($k_{ex} \approx 10{,}000\ s^{-1}$) with Ca^{2+}-bound TF-BAPTA[30] to be useful for generating iCEST contrast, we hypothesized that it could be used for the detection of other metal ions. Figure 1b shows the ^{19}F NMR spectrum of TF-BAPTA in the presence of either Zn^{2+} or Fe^{2+} (10:1 molar ratio). The $\Delta\omega$ of the ^{19}F atoms at 5- (purple) and 6-positions (green) are shifted downfield and upfield, respectively, in the presence of either of the ions, with a larger effect for the paramagnetic Fe^{2+}. One of the potential drawbacks of ^{19}F MRI using 5F-BAPTA is a possible line broadening of the bulk signal of the free ligand *in vivo* in live tissue,[19] such as seen when high amounts of Mg^{2+} are added (Figure S1, Supporting Information (SI)). As a result, images with reduced SNR may be experienced and smaller observed $\Delta\omega$ values may not be sufficient for selective saturation of poorly shifted nuclei without direct bulk saturation. However, as also previously demonstrated,[30] the fast exchange between Ca^{2+} and TF-BAPTA broadens the peak that is related to the 5-positioned ^{19}F atom and does not affect the NMR characteristics of the 6-positioned ^{19}F atom (Figure S2, SI). Additionally, a high Mg^{2+} concentration does not affect the NMR properties of 5F and 6F atoms of TF-BAPTA (Figure S2, SI), making the latter a suitable ^{19}F MRI probe in a biological setup. The 6-positioned ^{19}F atom for the signal of the bulk (in ^{19}F-CEST experiments) is thus preferable since it does not broaden due to ion exchange. The two frequencies that are observed in the ^{19}F NMR spectrum of TF-BAPTA require the center frequency offset (O_1) to be placed at the resonance of one of these frequencies when performing ^{19}F MRI. Therefore, all ^{19}F MRI experiments in this study were performed with O_1 set at the frequency of the 6-positioned ^{19}F, while the signal from the 5-positioned ^{19}F was suppressed using a spectrally selective excitation pulse and spoiler gradient.

Figure 2b,c shows the ^{1}H and ^{19}F MR images of seven tubes containing 10 mM TF-BAPTA and 200 μM added ion, without any observable changes in ^{1}H or ^{19}F MR contrast. However, the ^{19}F iCEST images show a clear differential MR contrast between the samples containing Zn^{2+} (Figure 2d) and Fe^{2+} (Figure 2e),

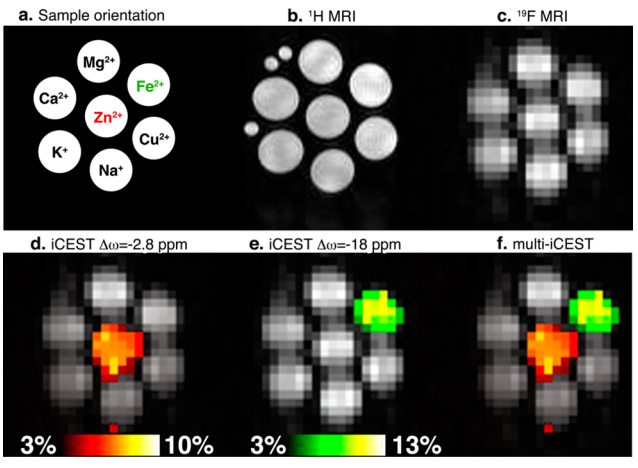

Figure 2. iCEST maps. (a) The orientation of the samples in the phantom containing 10 mM TF-BAPTA and 200 μM ion (pH = 7.2). (b) ^{1}H MRI, (c) ^{19}F MRI, (d) iCEST ($\Delta\omega = -2.8$ ppm) overlaid on ^{19}F MRI, (e) iCEST ($\Delta\omega = -18$ ppm) overlaid on ^{19}F MRI, and (f) both iCEST results ($\Delta\omega = -2.8$ ppm, $\Delta\omega = -18$ ppm) overlaid on ^{19}F MRI.

for a saturation pulse applied at $\Delta\omega = -2.8$ and -18 ppm, respectively. These $\Delta\omega$ values were chosen from the ^{19}F NMR spectra, using the offset values of TF-BAPTA upon the addition of Zn^{2+} or Fe^{2+}, respectively (see Figure 1b). Figure 2f clearly shows that both ions can be simultaneously visualized using TF-BAPTA as a single iCEST probe. Figure 3 shows the

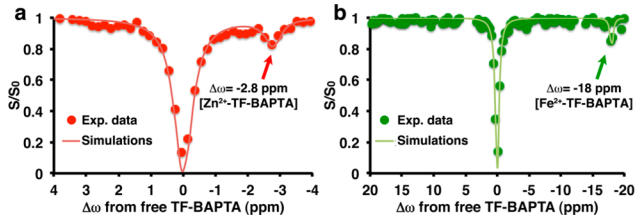

Figure 3. ^{19}F iCEST spectra for samples containing 10 mM TF-BAPTA and 200 μM Zn^{2+} (a) and Fe^{2+} (b). Circles represent experimental signal; solid lines represent Bloch simulations (two-pool model).

corresponding ^{19}F iCEST spectra for samples containing either Zn^{2+} (Figure 3a) or Fe^{2+} (Figure 3b). The dynamic ^{19}F exchange between TF-BAPTA and [M^{2+}-TF-FBAPTA] results in an iCEST effect for both ions, at $\Delta\omega = -2.8$ ppm for [Zn^{2+}-TF-BAPTA] and at $\Delta\omega = -18$ ppm for [Fe^{2+}-TF-BAPTA], respectively. Using Bloch simulations (Figure 3a,b), the exchange rate (k_{ex}) between free and bound TF-BAPTA is estimated to be $\sim 20\ s^{-1}$ for both ions. This k_{ex} is rather low, and much higher CEST contrast may be obtained for ^{19}F chelates with higher k_{ex} values. Despite this slow exchange, we were still able to detect 10% CEST contrast for a 200 μM ion concentration with the sensitivity from a 10 mM signal strength. The use of ^{19}F based CEST enables a reduction in the concentration of the ^{19}F iCEST probe to a biological relevant molar ratio (probe: ion), a feat that is not possible with ^{1}H CEST, which is based on water. Additionally, ^{19}F enables "hot spot" tracer detection without an endogenous background signal,[31] contrary to ^{1}H CEST, which suffers from a large nonspecific endogenous background signal. This may further reduce the ^{19}F probe concentration to below 10 mM, alleviating potential toxicity effects from Ca^{2+} buffering. Although TF-BAPTA did not show a significant buffering effect for intracellular Ca^{2+},[30] further studies are needed prior to its use *in vivo*. Importantly, when balanced salt solutions containing physiological levels of other ions (1.3 mM Ca^{2+}, 0.9 mM Mg^{2+}, 5.9 mM K^+, and 143 mM Na^+) and glucose (6 mM) were used, the iCEST effect from Zn^{2+} was not affected (Figure S3, SI). This is a great advantage for the use of TF-BAPTA as an iCEST probe compared to 5F-BAPTA, which exchanges much faster with other metal ions, causing broadening of the bulk signal in the ^{19}F NMR spectrum, limiting its applications.

The unique and different $\Delta\omega$ value of the exchangeable moiety is one of the most exceptional characteristics of iCEST compared to other MRI sensors. This feature gives CEST sensors an artificial color designation, by which they can be tagged in a singular specific frequency, much like fluorescent dyes. For ^{1}H CEST, this has been exploited for "multi-color" MRI of live cells[28] and *in vivo*.[27] Here (Figure 4) we investigated whether Zn^{2+} and Fe^{2+} could be distinguished from each other when mixed together and with other ions. When a saturation pulse was applied at the resonance of the Zn^{2+}-TF-BAPTA complex (i.e., $\Delta\omega = -2.8$ ppm), only the tubes that contained Zn^{2+} ions generated an observable iCEST contrast. The contrast did not change when competing ions, such as Ca^{2+}, Mg^{2+}, or Fe^{2+}, were

dx.doi.org/10.1021/ja511313k | J. Am. Chem. Soc. 2015, 137, 78−81

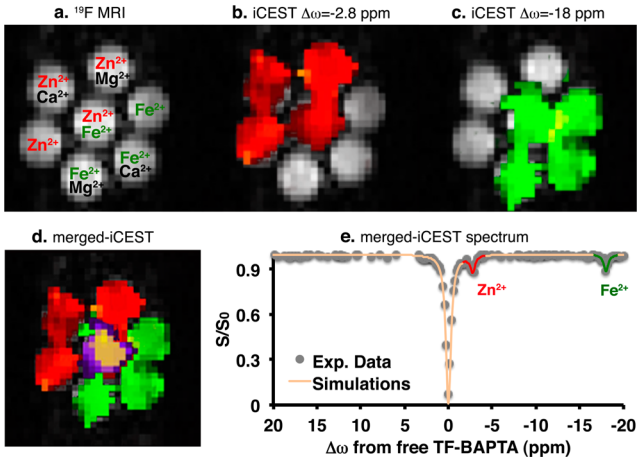

Figure 4. Simultaneous detection of multiple metal ions. (a) ^{19}F MRI and the orientation of the tubes in the phantom containing 10 mM of TF-BAPTA and 200 μM of mixed ions, (b) iCEST ($\Delta\omega$ = −2.8 ppm), and (c) iCEST ($\Delta\omega$ = −18 ppm) overlaid on ^{19}F MRI. (d) Merged iCEST image highlights (orange−purple scale) the shared iCEST contrast voxels shown in panels b and c. (e) ^{19}F iCEST spectra. Circles represent experimental signal; lines represent Bloch simulations (three-pool model).

included in the sample solution. Similarly, when the saturation pulse was applied at $\Delta\omega$ = −18 ppm ($\Delta\omega$ of Fe^{2+}-TF-BAPTA), only the samples that included Fe^{2+} generated iCEST contrast, without interference from the other coexisting ions Ca^{2+}, Mg^{2+}, or Zn^{2+}. Notably, when both Zn^{2+} and Fe^{2+} ions were mixed with TF-BAPTA (center tube in Figures 4a−d), the iCEST contrast could be obtained at both $\Delta\omega$ values of Zn^{2+}-TF-BAPTA (−2.8 ppm) and Fe^{2+}-TF-BAPTA (−18 ppm). The unique ability to detect two different ions using a single imaging probe (TF-BAPTA) is clearly reflected in the two distinctive peaks that were obtained in the iCEST spectra (Figure 4e). These experimental results were further supported by Bloch simulations using a three-pool model (Figure 4e).

The capability of detecting ^{19}F probes at sub millimolar concentrations,[32] the high sensitivity of the ^{19}F NMR spectrum $\Delta\omega$ values to changes in the chemical environment,[33] together with the frequency being specific of these $\Delta\omega$s for certain metal ions, should inspire further development of novel responsive contrast agents for iCEST MRI. One strategy that allows a local increase of the ^{19}F probe concentration and eliminating the need of systemic administration is to coencapsulate the imaging probe with the transplanted target cells.[39] For example, such an approach may be used for the detection of transplanted β cells that release Zn^{2+} upon the release of insulin.[12] By adding ^{19}F atoms to the two 6-positions of 5F-BAPTA (which previously allowed the detection of only Ca^{2+} using iCEST[29,34]) it became possible to detect both Zn^{2+} and Fe^{2+}. Adding one ^{19}F atom to the BAPTA backbone dramatically changes the binding properties of TF-BAPTA.[35] At the same time, the added ^{19}F atom induces k_{ex} values that allow the detection of Zn^{2+} and Fe^{2+} with ^{19}F iCEST MRI. Although other ^{1}H MRI probe can be used to detect Zn^{2+}[12,36−38] with a potential higher sensitivity as compared to ^{19}F probes, the specificity of iCEST to simultaneously detect different coexisting ions using the same sensor represents a new concept for the rational design of novel MRI probes. While BAPTA derivatives are widely used for the fluorescent detection of metal homeostasis *in vitro*, the possibility to probe metals *in vivo* noninvasively with MRI would have profound implications for the biological sciences.

■ ASSOCIATED CONTENT

Supporting Information

Experimental methods and figures. This material is available free of charge via the Internet at http://pubs.acs.org.

■ AUTHOR INFORMATION

Corresponding Author

*jwmbulte@mri.jhu.edu

Notes

The authors declare no competing financial interest.

■ ACKNOWLEDGMENTS

Supported by NIH R03EB018882, R01EB012590, and MSCRFII-0161-00.

■ REFERENCES

(1) Taylor, K. M.; Jin, A.; Lin, W. *Angew. Chem., Int. Ed.* **2008**, *47*, 7722.
(2) Cheng, L.; Yang, K.; Li, Y.; Chen, J.; Wang, C.; Shao, M.; Lee, S. T.; Liu, Z. *Angew. Chem., Int. Ed.* **2011**, *50*, 7385.
(3) Lee, J. H.; Lee, K.; Moon, S. H.; Lee, Y.; Park, T. G.; Cheon, J. *Angew. Chem., Int. Ed.* **2009**, *48*, 4174.
(4) Kim, J.; Piao, Y.; Hyeon, T. *Chem. Soc. Rev.* **2009**, *38*, 372.
(5) Niers, J. M.; Chen, J. W.; Lewandrowski, G.; Kerami, M.; Garanger, E.; Wojtkiewicz, G.; Waterman, P.; Keliher, E.; Weissleder, R.; Tannous, B. A. *J. Am. Chem. Soc.* **2012**, *134*, 5149.
(6) Rolfe, B. E.; Blakey, I.; Squires, O.; Peng, H.; Boase, N. R.; Alexander, C.; Parsons, P. G.; Boyle, G. M.; Whittaker, A. K.; Thurecht, K. *J. Am. Chem. Soc.* **2014**, *136*, 2413.
(7) Mbatia, H. W.; Burdette, S. C. *Biochemistry* **2012**, *51*, 7212.
(8) Carter, K. P.; Young, A. M.; Palmer, A. E. *Chem. Rev.* **2014**, *114*, 4564.
(9) Tsien, R. Y. *Biochemistry* **1980**, *19*, 2396.
(10) Tsien, R. Y. *Annu. Rev. Neurosci.* **1989**, *12*, 227.
(11) Garaschuk, O.; Milos, R. I.; Konnerth, A. *Nat. Protoc.* **2006**, *1*, 380.
(12) Lubag, A. J.; De Leon-Rodriguez, L. M.; Burgess, S. C.; Sherry, A. D. *Proc. Natl. Acad. Sci. U.S.A.* **2011**, *108*, 18400.
(13) Bar-Shir, A.; Avram, L.; Yariv-Shoushan, S.; Anaby, D.; Cohen, S.; Segev-Amzaleg, N.; Frenkel, D.; Sadan, O.; Offen, D.; Cohen, Y. *NMR Biomed.* **2014**, *27*, 774.
(14) Mamedov, I.; Canals, S.; Henig, J.; Beyerlein, M.; Murayama, Y.; Mayer, H. A.; Logothetis, N. K.; Angelovski, G. *ACS Chem. Neurosci.* **2010**, *1*, 819.
(15) Atanasijevic, T.; Shusteff, M.; Fam, P.; Jasanoff, A. *Proc. Natl. Acad. Sci. U.S.A.* **2006**, *103*, 14707.
(16) Dhingra, K.; Fouskova, P.; Angelovski, G.; Maier, M. E.; Logothetis, N. K.; Toth, E. *J. Biol. Inorg. Chem.* **2008**, *13*, 35.
(17) Li, W. H.; Fraser, S. E.; Meade, T. J. *J. Am. Chem. Soc.* **1999**, *121*, 1413.
(18) Kotera, N.; Tassali, N.; Leonce, E.; Boutin, C.; Berthault, P.; Brotin, T.; Dutasta, J. P.; Delacour, L.; Traore, T.; Buisson, D. A.; Taran, F.; Coudert, S.; Rousseau, B. *Angew. Chem., Int. Ed.* **2012**, *51*, 4100.
(19) Smith, G. A.; Hesketh, R. T.; Metcalfe, J. C.; Feeney, J.; Morris, P. G. *Proc. Natl. Acad. Sci. U.S.A.* **1983**, *80*, 7178.
(20) Tassali, N.; Kotera, N.; Boutin, C.; Leonce, E.; Boulard, Y.; Rousseau, B.; Dubost, E.; Taran, F.; Brotin, T.; Dutasta, J. P.; Berthault, P. *Anal. Chem.* **2014**, *86*, 1783.
(21) Harvey, P.; Chalmers, K. H.; De Luca, E.; Mishra, A.; Parker, D. *Chemistry* **2012**, *18*, 8748.
(22) van Zijl, P. C.; Yadav, N. N. *Magn. Reson. Med.* **2011**, *65*, 927.
(23) Hancu, I.; Dixon, W. T.; Woods, M.; Vinogradov, E.; Sherry, A. D.; Lenkinski, R. E. *Acta. Radiol.* **2010**, *51*, 910.
(24) Soesbe, T. C.; Wu, Y.; Sherry, A. D. *NMR Biomed.* **2013**, *26*, 829.
(25) Liu, G.; Song, X.; Chan, K. W.; McMahon, M. T. *NMR Biomed.* **2013**, *26*, 810.

(26) Castelli, D. D.; Terreno, E.; Longo, D.; Aime, S. *NMR Biomed.* **2013**, *26*, 839.
(27) Liu, G.; Moake, M.; Har-el, Y. E.; Long, C. M.; Chan, K. W.; Cardona, A.; Jamil, M.; Walczak, P.; Gilad, A. A.; Sgouros, G.; van Zijl, P. C.; Bulte, J. W.; McMahon, M. T. *Magn. Reson. Med.* **2012**, *67*, 1106.
(28) Aime, S.; Carrera, C.; Delli Castelli, D.; Geninatti Crich, S.; Terreno, E. *Angew. Chem., Int. Ed.*. **2005**, *44*, 1813.
(29) Bar-Shir, A.; Gilad, A. A.; Chan, K. W.; Liu, G.; van Zijl, P. C.; Bulte, J. W.; McMahon, M. T. *J. Am. Chem. Soc.* **2013**, *135*, 12164.
(30) Murphy, E.; Steenbergen, C.; Levy, L. A.; Gabel, S.; London, R. E. *J. Am. Physiol.* **1994**, *266*, C1323.
(31) Bulte, J. W. *Nat. Biotechnol.* **2005**, *23*, 945.
(32) De Luca, E.; Harvey, P.; Chalmers, K. H.; Mishra, A.; Senanayake, P. K.; Wilson, J. I.; Botta, M.; Fekete, M.; Blamire, A. M.; Parker, D. *J. Biol. Inorg. Chem.* **2014**, *19*, 215.
(33) Yu, J. X.; Kodibagkar, V. D.; Cui, W.; Mason, R. P. *Curr. Med. Chem.* **2005**, *12*, 819.
(34) Gilboa, H.; Chapman, B. E.; Kuchel, P. W. *NMR Biomed.* **1994**, *7*, 330.
(35) London, R. E.; Rhee, C. K.; Murphy, E.; Gabel, S.; Levy, L. A. *J. Am. Physiol.* **1994**, *266*, C1313.
(36) Lee, T.; Zhang, X. A.; Dhar, S.; Faas, H.; Lippard, S. J.; Jasanoff, A. *Chem. Biol.* **2010**, *17*, 665.
(37) Luo, J.; Li, W. S.; Xu, P.; Zhang, L. Y.; Chen, Z. N. *Inorg. Chem.* **2012**, *51*, 9508.
(38) Zhang, X. A.; Lovejoy, K. S.; Jasanoff, A.; Lippard, S. J. *Proc. Natl. Acad. Sci. U.S.A.* **2007**, *104*, 10780.
(39) Chan, K. W.; Liu, G.; Song, X.; Kim, H.; Yu, T.; Arifin, D. R.; Gilad, A. A.; Hanes, J.; Walczak, P.; van Zijl, P. C. M.; Bulte, J. W. M.; McMahon, M. T. *Nat. Mater.* **2013**, *12*, 268.